Environmental Pollution 244 (2019) 877–884

Contents lists available at ScienceDirect

Environmental Pollution

journal homepage: www.elsevier.com/locate/envpol

Chemical characteristics of airborne particles in Xi'an, inland China during dust storm episodes: Implications for heterogeneous formation of ammonium nitrate and enhancement of N-deposition☆

Can Wu [a, d], Gehui Wang [a, b, c, d, e, *], Cong Cao [a, d], Jianjun Li [a], Jin Li [a, d], Feng Wu [a], Rujin Huang [a], Junji Cao [a], Yongmin Han [a], Shuangshuang Ge [b], Yuning Xie [b], Guoyan Xue [b], Xinpei Wang [b]

[a] State Key Laboratory of Loess and Quaternary Geology, Key Lab of Aerosol Chemistry and Physics, Institute of Earth Environment, Chinese Academy of Sciences, Xi'an, 710061, China

[b] Key Lab of Geographic Information Science of the Ministry of Education, School of Geographic Sciences, East China Normal University, Shanghai, 210062, China

[c] Center for Excellence in Regional Atmospheric Environment, Institute of Urban Environment, Chinese Academy of Sciences, Xiamen, 361021, China

[d] University of Chinese Academy of Sciences, Beijing, 100049, China

[e] School of Human Settlements and Civil Engineering, Xi'an Jiaotong University, Xi'an, 710049, China

A R T I C L E I N F O

Article history:
Received 16 June 2018
Received in revised form
3 October 2018
Accepted 3 October 2018
Available online 29 October 2018

Keywords:
Asian dust
Size distributions
Composition
Source
Nitrogen deposition

A B S T R A C T

To identify the sources and heterogeneous reactions of sulfate and nitrate with dust in the atmosphere, airborne particles in Xi'an, inland China during the spring of 2017 were collected and measured for chemical compositions, along with a laboratory simulation of the heterogeneous formation of ammonium nitrate on the dust surface. Our results showed that concentrations of Ca^{2+}, Na^+ and Cl^- in the TSP samples were enhanced in the dust events, with the values of 41.8, 5.4 and 4.0 μg m^{-3}, respectively, while NO_3^- (7.1 μg m^{-3}) and NH_4^+ (2.4 μg m^{-3}) remarkably decreased, compared to those in the non-dust periods. During the dust events, NH_4^+ correlated only with NO_3^- ($R^2 = 0.52$) and abundantly occurred in the coarse mode (>2.1 μm), in contrast to that in the non-dust periods, which well correlated with sulfate and nitrate and enriched in the fine mode (<2.1 μm). SO_4^{2-} in Xi'an during the dust events existed mostly as gypsum ($CaSO_4{\cdot}2H_2O$) and mirabilite ($Na_2SO_4{\cdot}10H_2O$) and dominated in the coarse mode, suggesting that they were directly transported from the upwind Gobi Desert region. Our laboratory simulation results showed that during the long-range transport hygroscopic salts in the Gobi dust such as mirabilite can absorb water vapor and form a liquid phase on the particle surface, then gaseous NH_3 and HNO_3 partition into the aqueous phase and form NH_4NO_3, resulting in the strong correlation of NH_4^+ with NO_3^- and their accumulation on dust particles. The dry deposition flux of total inorganic nitrogen ($NH_4^+ + NO_3^-$) in Xi'an during the dust events was 0.97 mg-N m^{-2} d^{-1} and 37% higher than that in the non-dust periods. Such a significant enhanced N-deposition is ascribed to the heterogeneous formation of NH_4NO_3 on the dust particle surface, which has been ignored and should be included in future model simulations.

1. Introduction

Dusts are the major components of airborne particles in the atmosphere and take significant impacts on climate change directly by scattering and absorbing solar and terrestrial radiation (Huang et al., 2015; Li et al., 1996) and indirectly by influencing the formation and properties of clouds through serving as cloud condensation nuclei (CCN) (Karydis et al., 2011; Kumar et al., 2009; Tsai et al., 2015; Zhang et al., 2009) and ice nuclei (IN) (Creamean et al., 2013; Zimmermann et al., 2008). Per the fourth report of the Intergovernmental Panel on Climate Change (IPCC), the total direct radiative forcing of dust aerosols was estimated to

☆ This paper has been recommended for acceptance by Joerg Rinklebe.

* Corresponding author. Key Lab of Geographic Information Science of the Ministry of Education, School of Geographic Sciences, East China Normal University, Shanghai, 210062, China.

E-mail addresses: ghwang@geo.ecnu.edu.cn, wanggh@ieecas.cn (G. Wang).

https://doi.org/10.1016/j.envpol.2018.10.019
0269-7491/

be $-0.1 \pm 0.2\ W\ m^{-2}$ (Forster et al., 2007). Because they contain abundant iron, nitrogen and phosphorus, deposited dust particles during the long-range transport process could significantly influence the downwind ocean primary productivity and biogeochemical cycles (Chien et al., 2016; Jickells et al., 2005; Wang et al., 2017b). Also, dust particles can strongly reduce atmospheric visibility (Mahowald et al., 2007; Wang et al., 2012; Wang et al., 2013a) and cause human health problem, especially for those patients who suffer from respiratory and cardiac-cerebral vascular disease (Higashi et al., 2014; Meng and Lu, 2007; Tao et al., 2012).

The desert and Gobi areas in Mongolia and northern China are the major source regions of East Asia dust (Sun et al., 2010; Wang et al., 2017a; Zhao et al., 2015). Each year around 800 Tg dust particles from the regions are pumped out into the atmosphere, which accounts for over 50% of the global atmospheric dust (Zhang et al., 1997). The Asia dust can spread thousands of kilometers downwind over the east coastal China (Fu et al., 2010; Li et al., 2017; Zhao et al., 2011), Korea (Fu et al., 2010; Geng et al., 2014), Japan (Lee et al., 2015; Pan et al., 2015), North Pacific Ocean (Wu et al., 2015), and even arrive in the USA (Creamean et al., 2013), exerting a profound impact on the atmospheric environment over these regions. During the long-rang transport, the physicochemical properties of the dust particles could be changed by mixing with anthropogenic emissions (Fairlie et al., 2010; Li and Shao, 2009; Ma et al., 2012; Sun et al., 2004; Tang et al., 2010). For example, Tsai et al. (2015) found that the East Asia dust could become the effective CCN with an increase from around $10^7\ m^{-3}$ to more than $10^9\ m^{-3}$ over the downwind north Pacific regions. Adsorption or condensation of nitric acid on $CaCO_3$-containing particles may form more hygroscopic $Ca(NO_3)_2$, which would significantly change the dust aerosol hygroscopicity (Li et al., 2014a). Pan et al. (2015) revealed that the morphology of dust particles also varied during the long-range transport due to the impact of anthropogenic pollutants. In addition, the dust particles are effective carrier through coating the pollutants on the surface, of which the carrying ability is related to their sizes, shapes, and chemical composition (Nie et al., 2012; Wang et al., 2013a).

Xi'an is an inland metropolitan city in China and near the East Asia dust region. High level of particle pollution has been a persistent problem of the city not only due to the large emission of anthropogenic pollutants but also due to the significant input of dust from the upwind desert regions especially in spring (Li et al., 2016; Wang et al., 2016). In the past decade a few studies about dust storm in inland China including Xi'an have focused on PM mass concentrations, composition, and the health risks (Li et al., 2008; Li et al., 2014b; Shen et al., 2009), but poor knowledge is available for the aging process of dust aerosols such as the heterogeneous reactions of dust with pollutants. In this study, atmospheric TSP aerosol samples in Xi'an were collected with a 2-h time resolution during the 2017 spring dust storm events to explore the interactions of dust with anthropogenic emissions. We firstly investigated the changes in chemical compositions and size distributions of airborne particle in Xi'an due to the occurrence of the dust storm, then we identified the mechanism of ammonium nitrate accumulated on the dust particles, and finally we quantified the impact of the dust storm on the N-deposition in the city.

2. Experimental section

2.1. Sample collection

The TSP samples with a 2-h interval were collected by using a TCH-1000 air sampler during the three dust storm events (23 March to 25 March; 16 April to 18 April and 5 May to 7 May) on the campus of the Institute of Earth Environment, CAS (34.22 ºN, 108.88 ºE), which located in the urban center of Xi'an, inland China. Meanwhile, size-segregated samples were also collected using an Andersen impactor sampler, of which the cutoff points at an airflow rate of $28\ L\ min^{-1}$ were 0.43, 0.65, 1.1, 2.1, 3.3, 4.7, 5.8, and 9.0 μm, respectively. Each set of the size-resolved samples were collected for 9 h. Those samples could perfectly reflect the size distribution of TSP (S Fig. 1). All the filter samples were collected onto precombusted quartz filter (450 °C for 6 h). Concentrations of inorganic ions in $PM_{2.5}$ were measured with a 1-h time resolution by using In-situ Gas and Aerosol Compositions Monitor (IGAC). Detailed description of IGAC was reported by Young et al. (2016). To reveal the characteristics of individual dust particles, several TSP samples were collected onto polycarbonate filters at an airflow rate of $5\ L\ min^{-1}$ for 15 min during dust storm periods for morphology and elemental composition analysis by using Scanning Electronic Microscopy (SEM) (Li and Shao, 2009).

2.2. Chemical analysis

2.2.1. Inorganic ions analysis

One-eighth of each TSP sample was extracted three times under sonication with 15 ml Milli-Q pure water (18.2 MΩ). Ten of anions and cations (SO_4^{2-}, NO_3^-, Cl^-, NO_2^-, F^-, NH_4^+, Na^+, K^+, Mg^{2+} and Ca^{2+}) in the samples were analyzed by using an ion chromatography (Dionex, ICS-1100). The detailed analysis protocol was reported elsewhere (Wang et al. (2014).

2.2.2. Single particle analysis by scanning electronic microscopy (SEM)

Detailed procedure of the SEM analysis was reported by Li and Shao (2009). Briefly, dust particles on the polycarbonate filter were treated by spray-gold and were investigated by using a scanning electron microscope with the help of energy dispersive X-ray spectrometer (SEM-EDX, EVO 18 Research). The photos and energy spectrums of the particles were obtained at an accelerating voltage of 20 keV, which was beneficial to the studies of particle morphology, size, and elemental composition.

2.3. Mass concentrations of $PM_{2.5}$ andPM_{10} and meteorological data

Mass concentrations of $PM_{2.5}$ and PM_{10} during the sample periods were downloaded from the website of Chinese air quality online monitoring analysis platform (http://www.aqistudy.cn). Meteorological data of Xi'an were obtained from the Shaanxi Meteorological Bureau (Fig. 1).

2.4. Potential source contribution function (PSCF) analysis

PSCF is a useful method to identify the potential spatial sources of aerosols based on tracing the air mass history pathway and the measured concentration of aerosols (Argyropoulos et al., 2017; Young et al., 2016). 24-h air mass back trajectories are calculated by using Hybrid-Single Particle Lagrangian Integrated Trajectory model, developed by the National Oceanic and Atmospheric Administration's (NOAA) Air Resources Laboratory (ARL) (http://www.arl.noaa.gov/ready/hysplit4.html). The PSCF analysis was conducted by TrajStat, a free software developed by Wang et al. (2009).

2.5. Calculation of nitrogen dry deposition flux

The dry deposition flux is directly proportional to the local concentration C of the depositing species.

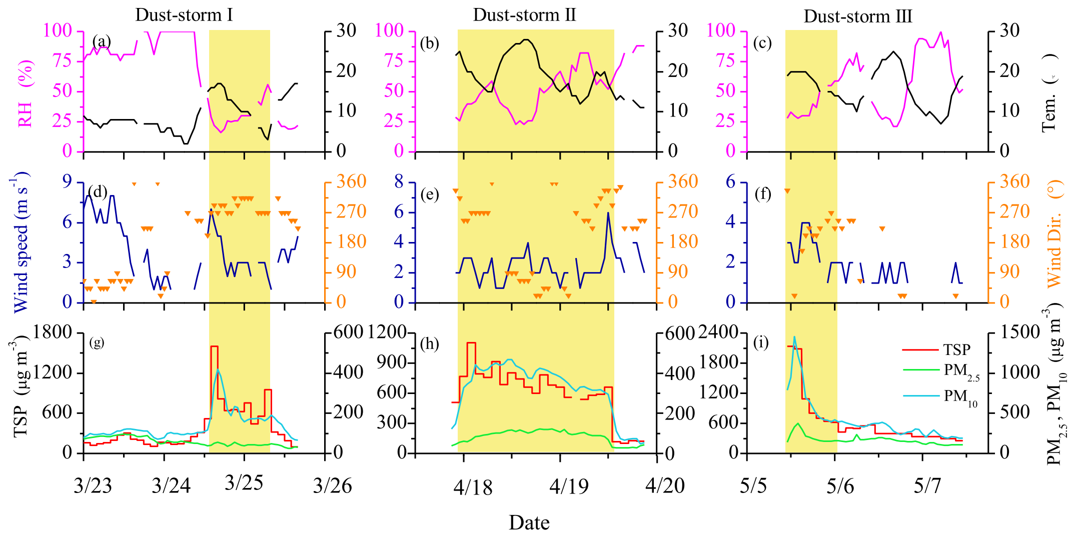

Fig. 1. Temporal variations of TSP, PM_{10}, $PM_{2.5}$ and meteorological parameters during the sampling period. Dust storm I, II, and III were the three dust events, respectively (yellow shadows indicating the dust storm events). (For interpretation of the references to colour in this figure legend, the reader is referred to the Web version of this article.)

$$F = v_d C \tag{1}$$

Where F is the vertical dry deposition flux μg $m^{-2}\,s^{-1}$, v_d is the deposition velocity m s^{-1}, C is the concentration of the aerosol, the deposition velocity v_d can be expressed as (Seinfeld and Pandis, 1998):

$$v_d = \frac{1}{\gamma_a + \gamma_b + \gamma_a \gamma_b v_s} + v_s \tag{2}$$

Where γ_a is the aerodynamic resistance above the canopy, γ_b is the quasi-laminar layer resistance, v_s is the settling velocity, which is calculated as follows:

$$v_s = \frac{\rho_p dp^2 g C_C}{18\mu} \tag{3}$$

where ρ_p is the density of the particle, Cc is the slip correction coefficient, μ is the viscosity of air and can be calculated as 1.8×10^{-5} $(T/298)^{0.85}$. The aerodynamic resistance for particle can be calculated as $\ln(z_r/z_0)/\kappa u_*$, where z_r is the height at which the dry deposition velocity v_d is evaluated, z_0 is the roughness length, κ is the Von Karman constant and u_* is the friction velocity. The quasi-laminar resistances can be expressed as $1/\varepsilon_0 u_*(E_B + E_{IM} + E_{IN})\, R_1$, ε_0 is an empirical constant = 3.0. E_B is represented as $S_C^{-\gamma}$, the values of γ are relevant to different land-use categories, S_C is Schmidt number. E_{IM} is expressed as $(St/(St+\alpha))^{\beta}$, where α depends on the land use category and β = 2, St is Stokes number. E_{IN} adapted here is $0.5(dp/A)^2$. Finally, the parameter R_1 represents the fraction of particles, which can be calculated as $\exp(-St^{1/2})$.

3. Results and discussion

3.1. General description of the dust events and potential sources

Fig. 1 shows the temporal variations of meteorological parameters and particle concentrations observed in Xi'an during the spring of 2017. The dust periods were highlighted by the yellow shadow in Fig. 1 with 2-h TSP concentration higher 600 μg m^{-3}, and meteorological characteristic coincided with passage of the cold front (Hu et al., 2016). Three dust events occurred in the city during the campaign, with hourly TSP concentrations peaking at 1600, 1103, and 2136 μg m^{-3}, respectively. PM_{10} and $PM_{2.5}$ showed similar temporal variation patterns during the observation. Dust concentrations simulated by NAAPS (https://www.nrlmry.navy.mil/) also showed that there were three dust plumes arriving in Xi'an during the sampling periods (Fig. S2). In the dust storm periods, TSP ranged from 446 to 2136 μg m^{-3} with an average of 808 ± 387 μg m^{-3}, which is 3.3 times higher than that during the non-dust storm periods (Table 1). PM_{10} and $PM_{2.5}$ during dust storm periods were 407 ± 231 and 107 ± 67 μg m^{-3}, respectively. The ratio of $PM_{2.5}$/TSP decreased significantly from 35 ± 14% in the non-dust storm period to 13 ± 5.4% in the dust-storm events (Table 1), but the absolute concentration (107 ± 67 μg m^{-3}, Table 1) of $PM_{2.5}$ in the dust storm periods are comparable and even higher than that (94 ± 52 μg m^{-3}, Table 1) in the non-dust storm periods, suggesting the abundant occurrence of fine particles in Asian dust storm periods.

To explore the sources and transport pathways of the dust plumes, PSCF analysis was applied in this study. As shown in Fig. S3, the transport pathways of the three dust plumes can be classified as two types. One was originated from the Gobi Desert of Gansu Province, China, transported toward the southeast and then reached Xi'an, and the other one was originated from Gobi Desert of Mongolian, moved across Inner Mongolia, Ningxia and arrived in Xi'an. The transport tracks were slightly different, but all of them passed through the Tengger Desert and Badan Jaran Desert, both of which are the major source regions of Asian dust (Wang et al., 2017a; Zhang et al., 1997). The higher PSCF values demonstrated that the two deserts were the main sources of TSP in Xi'an during the three dust storm events.

3.2. Characteristics of water-soluble ions

As shown in Table 1, the concentrations of Ca^{2+}, Mg^{2+}, K^+ and Na^+ during the dust storm periods were 1–3 times higher than those in the non-dust storm periods due to their crustal origins (Shen et al., 2009; Wang et al., 2014). In the dust storm events, Ca^{2+} was the most abundant ion in TSP (Fig. 2a), accounting for 53.4% of the total ions, followed by SO_4^{2-} (17.4%) and NO_3^- (9.5%). Na^+, Cl^- and NH_4^+ were relatively low, accounting for 6.5%, 5.0% and 3.3% of the total, respectively. SNA (sulfate, nitrate and ammonium) during

Table 1
Concentrations (μg m^{-3}) of inorganic ions in TSP and meteorological conditions during the dust storm and non-dust storm periods of 2017 in Xi'an, inland China.

	Dust storm		Non-dust storm	
	Average ± SD	Range	Average ± SD	Range
I. Inorganic ions in TSP samples				
F^-	0.54 ± 0.37	0.2–2.4	0.44 ± 0.27	0.12–1.32
Cl^-	4.0 ± 2.8	1.4–14.0	3.4 ± 2.0	1.4–10.9
NO_3^-	7.1 ± 2.8	3.7–14.9	15.7 ± 10.5	4.8–33.8
SO_4^{2-}	14.8 ± 6.8	8.1–39.2	16.2 ± 8.7	5.2–33.0
Na^+	5.4 ± 3.1	2.1–17.5	3.2 ± 1.8	0.9–8.6
NH_4^+	2.4 ± 1	0.9–4.5	10.5 ± 8.5	1.5–24
K^+	1.4 ± 2.0	0.1–12.4	1.4 ± 1.0	0.3–5.5
Mg^{2+}	2.0 ± 1.1	0.9–5.8	0.7 ± 0.5	0.2–1.9
Ca^{2+}	41.8 ± 18.7	27.4–98.8	14.0 ± 8.8	2.6–31.1
II. TSP, PM_{10} and $PM_{2.5}$				
TSP	808 ± 387	446–2136	248 ± 132	98–573
PM_{10}	407 ± 231	152–1457	179 ± 107	49–417
$PM_{2.5}$	107 ± 67	36–378	94 ± 52	25–232
$PM_{2.5}$/TSP (%)	13.0 ± 5.4	3.3–24.1	35.0 ± 14.0	12.0–67
III. Meteorological parameters				
Temperature (T, °C)	17.5 ± 5.3	4.0–28	11.5 ± 5.7	2.0–25
Relative humidity (RH, %)	42.0 ± 17.0	16–82	70 ± 25	19–100
Wind speed (WS, m s^{-1})	2.6 ± 1.1	1.0–7.0	3.0 ± 2.1	1.0–8.0

the non-dust periods increased significantly in TSP compared to those in the dust storm events, accounting for 58.7% of the total (Fig. 2b). Although Ca^{2+} was the most abundant ion (26%) during the non-dust storm periods, the concentration of NH_4^+ was remarkably enhanced by a factor of 4.7 (Table 1). The small pie charts in Fig. 2 show the relative abundance of individual ion to the total ions in $PM_{2.5}$. For the fine particle, concentrations of Ca^{2+}, NO_3^- and NH_4^+ varied significantly when dust storm occurred. As seen in Fig. 2, Ca^{2+} was the most abundant cation in the dust storm periods and two times higher than that in the non-dust storm periods. On the contrary, the fine particulate NO_3^- and NH_4^+ during the dust storm events were quite low and only about half of those in the non-dust periods.

During the dust periods, SO_4^{2-} robustly correlated with Ca^{2+}, Na^+, Mg^{2+} and K^+ but not correlated with NH_4^+ (Table S1), indicating that SO_4^{2-} may exist in the form of $CaSO_4$, Na_2SO_4. To confirm this speculation, a SEM-EDX technique was used to analyze the chemical compsition of the dust. As shown in Fig. 3, particles collected during the dust periods can be classfied as two types. One type is composed by calcium, sulfur, carbon and oxygen, suggesting that the dust particles are $CaCO_3$ and $CaSO_4$; another type is composed by calcium, sodium, carbon and oxygen, indicating that the dust particles are $CaCO_3$ and Na_2SO_4, those particles accounted for 16.7% of the total (126 particles) analyzed by SEM-EDX. Similar result was also found in Qingdao, China (Niu et al., 2016). Mirabilite mines ($Na_2SO_4 \cdot 10H_2O$) and salt lakes widely distribute along the dust storm transport pathways (Fig. S4). The significant amount of Na_2SO_4 in the dust samples further demonstrates that sulfate in Xi'an during the dust periods was mostly transported from the desert surface soil rather than secondarily produced by photochemical oxidation of SO_2. Therefore, high correlations were found for SO_4^{2-} with Ca^{2+}, Na^+, K^+ and Mg^{2+}. In contrast, in the dust storm events NO_3^- only showed a strong correlation with NH_4^+ (Table S1), indicating both were secondarily formed via a common pathway, which will be discussed in section 3.4.

3.3. *Size distributions of major ions*

Fig. 4 illustrates the size distributions of major ions during the dust and non-dust periods, respectively. Ca^{2+} and Na^+ are crustal species and thus dominated in the coarse mode during the dust and the non-dust periods. NH_4^+ presented bimodal pattern during the dust storm periods with a significant amount in the coarse mode (>2.1 μm) (Fig. 4a, c and e), in contrast to that in the non-dust storm events, which peaked in the fine mode (<2.1 μm) (Fig. 4g), further implying that NH_4^+ aerosols in the dust storm and non-dust storm periods were formed via different pathways.

During the dust storm periods, SO_4^{2-}, NO_3^- and Cl^- exhibited

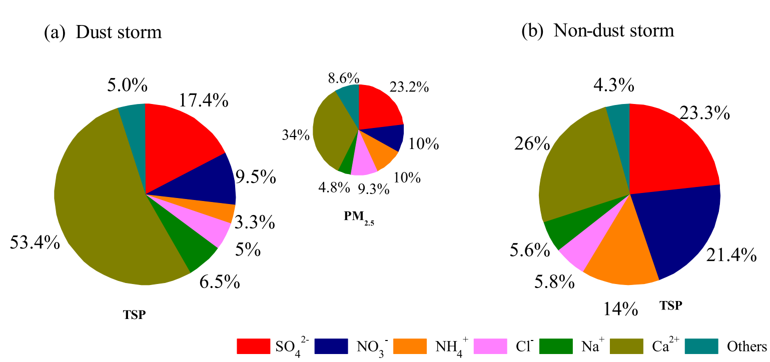

Fig. 2. Percentages of individual ion to the total ions in TSP and $PM_{2.5}$ during (a) the dust storm and (b) the non-dust storm period.

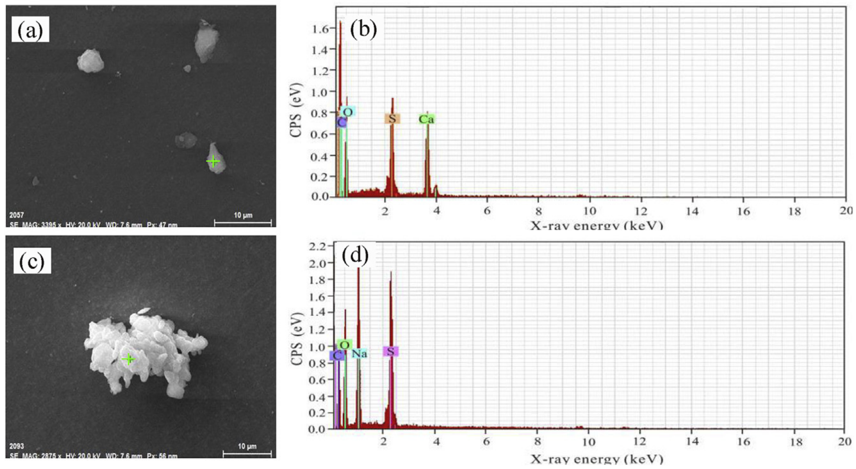

Fig. 3. SEM images and EDX spectra of the coarse particles collected during the dust storm periods ((a) and (b) "Ca & S-dominant", mainly composed of $CaSO_4$, (c) and (d) "Na & S-dominant", mainly composed of Na_2SO_4).

unimodal pattern, peaking at the coarse mode (>2.1 μm). The size distribution pattern of SO_4^{2-} was similar to that of Cl^- but different from NO_3^- (Fig. 4b, d and f), because both SO_4^{2-} and Cl^- were directly transported from the desert regions to the sampling site (Wang et al., 2014). During the non-dust storm periods those, anions displayed a bimodal size distribution, peaking at 0.43–0.67 μm and >2.1 μm, respectively (Fig. 4h).

3.4. The formation mechanism of nitrate and ammonium aerosols during dust periods

As shown in Fig. 5, the average mass ratio of SO_4^{2-}/TSP was 1.8% at the sampling site and slightly higher than that (average, 1.2%) in TSP collected at Tengger Desert. Such a result is consistent with the study by Wu et al. (2017). In contrast, the average ratios of NO_3^-/TSP and NH_4^+/TSP in Xi'an were remarkably higher than those in the desert source regions. The abundance of NO_3^- and NH_4^+ relative to TSP in Shanghai (Wang et al., 2013b) and Jeju Island, Korea (Kang et al., 2009) were much higher than that in the desert area (Fig. 5), indicating the continuous formation of NO_3^- and NH_4^+ on the dust surface during the long-range transport. NO_3^- could be produced on carbonate-containing dust particles as $Ca(NO_3)_2$ via the heterogeneous reactions of $CaCO_3$ with HNO_3 and N_2O_5. Thus, a strong correlation of NO_3^- with Ca^{2+} has often been observed during the dust storm periods (Li and Shao, 2009; Tang et al., 2016).

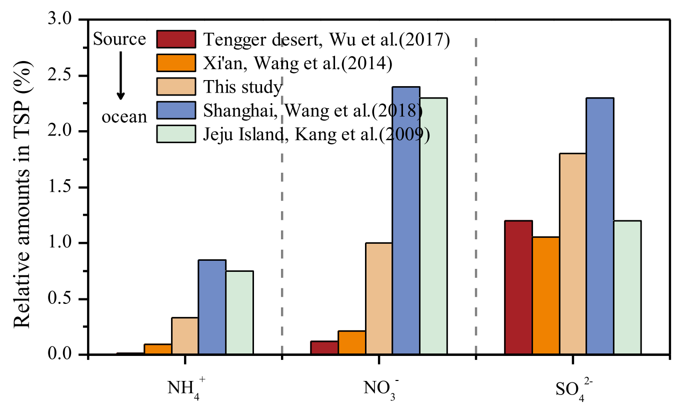

Fig. 5. A comparison on the relative abundances of SO_4^{2-}, NO_3^- and NH_4^+ in dust particles during the long-range transport from the upwind regions (Tengger Desert and Xi'an city) to the downwind regions (Shanghai city, China and Jeju Island, Korea).

However, such a correlation was not observed in the current work. Instead, we found that NO_3^- displayed a robust linear correlation only with NH_4^+ during the dusty periods (Table S1), indicating that both mainly existed as NH_4NO_3.

According to above discussion, here we propose a heterogeneous formation pathway to explain the cooccurrence of NO_3^- and

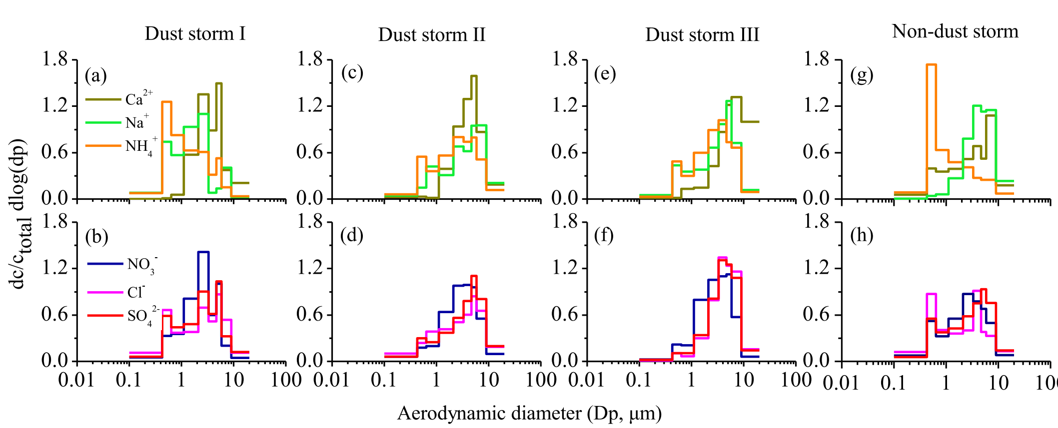

Fig. 4. Size distributions of airborne particulate ions in Xi'an, inland China during the dust storm and non-dust-storm periods.

NH_4^+ on the dust particle surface. As shown in Fig. 6, dust particles containing-mirabilite take up water vapor from the surrounding air during the transport process and form a liquid phase on the particle surface, because Na_2SO_4 is a hygroscopic salt. Then gaseous HNO_3 and N_2O_5 partition into the liquid phase and produce nitric acid. The nitric acid solution on the dust surface is further neutralized by the gas phase ammonia to produce NH_4NO_3, resulting in the accumulation of NH_4^+ on the coarse mode particles.

To verify the conceptual model and interpret the accumulated NH_4^+ on the dust particle surface, we conducted a series of laboratory experiments by exposing the Na_2SO_4 particles to the gaseous HNO_3(g) and NH_3(g) under humid conditions (RH > 90%) in a reaction cell. After for a 3–6 h exposure, the Na_2SO_4 particles in the reaction cell were collected and analyzed using ion chromatography. The results showed that a considerable amount of NH_4^+ was detected in the Na_2SO_4 solution with a molar ratio of 0.02 for NH_4^+/Na^+ (Fig. S5). In contrast, the NH_4^+/Na^+ molar ratio in the solution was less than 0.005 either under a dry condition (RH < 20%) or in the absence of gaseous HNO_3, confirming the heterogeneous formation mechanism we proposed for the coarse mode of NH_4NO_3 in Xi'an during the dust events.

3.5. Nitrogen dry deposition enhanced by NH_4NO_3 formation

Nitrogen, as the essential nutrient, is useful for all life form in the terrestrial and aquatic ecosystems, but excessive nitrogen also poses many serious environmental problems such as eutrophication, soil acidification, altering biological diversity (Clark and Tilman, 2008; Fang et al., 2011; Liu et al., 2011; Vitousek et al., 1997). The main source of the N on the Earth surface soil is the dry deposition, which contributes up to two-thirds of total N deposition (Flechard et al., 2011; Vet et al., 2014). As discussed in section 3.3, NO_3^- and NH_4^+ during dust periods have a tendency to accumulate in the coarse mode and is thus easier to deposit than those in the fine mode due to the gravity. Therefore, it would be of different deposition characteristics compared to those in the non-dust storm periods. Since NO_3^- and NH_4^+ almost entirely distribute in the size range of <9.0 µm, the analysis upon nitrogen dry deposition in the current work focus on those fractions.

The dry deposition flux can be estimated from equation (1) in section 2.5, while dry deposition velocities for the individual species are obtained by the following equation (Caffrey et al., 1998; Shi et al., 2013):

$$V_d = \frac{\sum_{i=1}^{n} V_i \bullet C_{i,a}}{\sum_{i=1}^{n} C_{i,a}} \tag{4}$$

Where V_i and $C_{i,a}$ are the deposition velocity and the average mass concentration of ion species in the ith size range, respectively.

Table 2
The dry deposition velocity and flux of NO_3^- and NH_4^+ during dust and non-dust period.

	Dust periods	Non-dust periods
I. Deposition velocity V_d (cm s^{-1})		
NO_3^-	0.17 ± 0.02	0.15 ± 0.02
NH_4^+	0.17 ± 0.02	0.13 ± 0.03
II. Dry deposition flux (mg m^{-2} d^{-1})		
NO_3^-	0.78 ± 0.18	0.56 ± 0.17
NH_4^+	0.19 ± 0.03	0.15 ± 0.10
TIN[a]	0.97 ± 0.18	0.71 ± 0.21

[a] TIN = NO_3^- + NH_4^+.

During the non-dust storm periods, the deposition velocities of NO_3^- and NH_4^+ in Xi'an were estimated to be 0.16 ± 0.02 and 0.14 ± 0.03 cm s^{-1}, respectively (Table 2). The calculated value of NO_3^- is in a good agreement with that reported by Xu et al. (2015) over China (0.17 cm s^{-1}) and Liu et al. (2017) in Chinese urban area (0.18 cm s^{-1}). However, the deposition velocity calculated for NH_4^+ is slightly lower than the value of 0.17 cm s^{-1} reported by Liang et al. (2016) in Shaanxi Province, China. Such a difference is probably resulted from the difference in meteorological conditions during the different sampling periods (Mohan, 2016). In comparison with those in the non-dust storm periods higher deposition velocities are obtained for all the ions during the dust storm periods, of which NH_4^+ and NO_3^- present a same deposition velocity (0.17 ± 0.02 cm s^{-1}). The higher V_d during the dust storm periods in Xi'an could be explained by the higher percentage of coarse particle and the larger wind speed (Yan et al., 2014).

The dry deposition flux of TIN (a sum of $NO_3^-$and NH_4^+) in Xi'an during the non-dust storm periods was calculated to be 0.71 ± 0.21 mg m^{-2} s^{-1} (Table 2), which is comparable with that (0.63 mg m^{-2} s^{-1}) reported by Xu et al. (2015) over Northwest China. In the current work, NO_3^- is the primary species for N-deposition flux, which is consistent with the results observed in Beijing and Tianjin (Pan et al., 2012). Compared to the non-dust storm periods, the deposition flux of TIN in the dust events in Xi'an was enhanced by a factor of 1.4, indicating that more N–nutrients would settle down in the farmland and open waters. Moreover, the deposition flux of coarse fraction during the dust periods is significantly higher than that in the non-dust storm period especially the NH_4^+–N (Fig. 7), leading to about 1 T d^{-1} of additional nitrogen during the dust storm periods deposited in the Xi'an urban area (10^3 km^2) in comparison with that in the non-dust storm periods. Such an enhanced N-deposition is caused by the heterogeneous formation of NH_4NO_3 on the mirabilite-containing coarse particles.

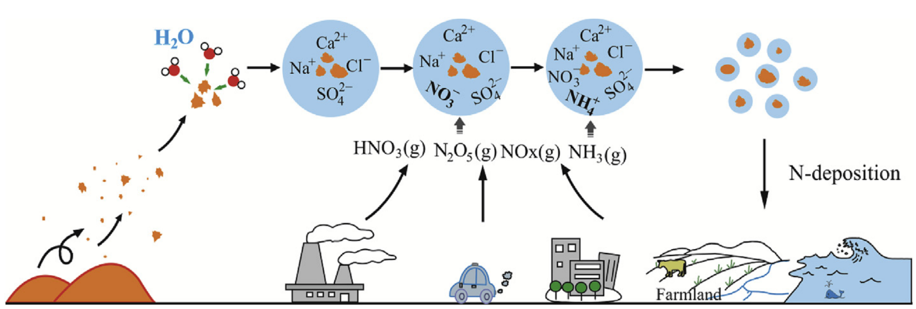

Fig. 6. A schematic diagram describing the heterogeneous formation of NH_4NO_3 on the dust surface during the long-range transport process.

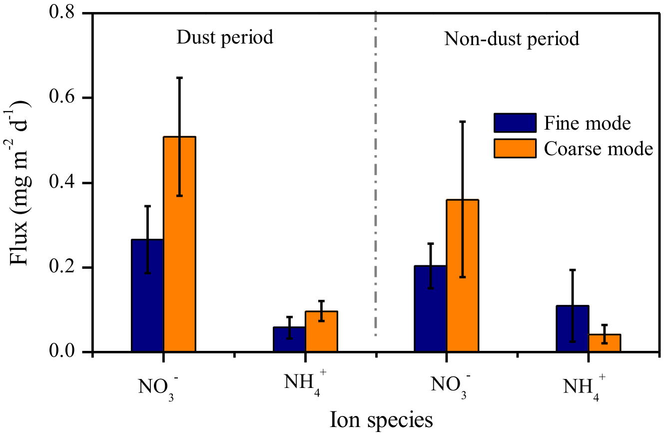

Fig. 7. The dry deposition flux of NO_3^- and NH_4^+ in the fine (<2.1 μm) and coarse (>2.1 μm) modes during the dust storm events of 2017 in Xi'an, inland China.

4. Conclusions

Airborne particles during the three dust storm events in Xi'an were characterized for chemical composition, formation mechanism, size distribution and N-deposition. During the dust storm periods SO_4^{2-} robustly correlated with Ca^{2+}, Na^+, Mg^{2+} and K^+, while NO_3^- merely correlated with NH_4^+. SEM-EDX analysis showed that in the dust periods SO_4^{2-} mostly existed in the form of Na_2SO_4 and $CaSO_4$, which were directly transported from the Gobi Desert regions. Size distribution results further showed that NO_3^- and NH_4^+ were enriched in the coarse mode (>2.1 μm) during the dust storm periods and existed as NH_4NO_3. Based on the field measurements and the laboratory simulation, we proposed a heterogeneous formation pathway to explain the cooccurrence of NO_3^- and NH_4^+ in the dust storm events, in which nitric acid was formed via partitioning of HNO_3 and N_2O_5 into the liquid phase of hygroscopic salts like mirabilite and was further neutralized by ammonia to produce NH_4NO_3, resulting in the accumulation of NH_4^+ on the coarse mode of particles. Such an accumulation of NH_4NO_3 on the dust particles enhanced the N-deposition, leading to about 1 T d^{-1} of additional nitrogen deposited in the urban area of Xi'an during the dust storm periods in comparison with that in the non-dust storm periods.

Acknowledgements

This work was financially supported by National Key R&D Plan (Quantitative Relationship and Regulation Principle between Regional Oxidation Capacity of Atmospheric and Air Quality (No. 2017YFC0210000), the China National Natural Science Funds for Distinguished Young Scholars (No.41325014), the program from National Nature Science Foundation of China (No. 41773117).

Appendix A. Supplementary data

Supplementary data to this article can be found online at https://doi.org/10.1016/j.envpol.2018.10.019.

References

Argyropoulos, G., Samara, C., Diapouli, E., Eleftheriadis, K., Papaoikonomou, K., Kungolos, A., 2017. Source apportionment of PM_{10} and $PM_{2.5}$ in major urban Greek agglomerations using a hybrid source-receptor modeling process. Sci. Total Environ. 601, 906–917.
Caffrey, P.F., Ondov, J.M., Zufall, M.J., Davidson, C.I., 1998. Determination of size-dependent dry particle deposition velocities with multiple intrinsic elemental tracers. Environ. Sci. Technol. 32, 1615–1622.
Chien, C.-T., Mackey, K.R.M., Dutkiewicz, S., Mahowald, N.M., Prospero, J.M., Paytan, A., 2016. Effects of African dust deposition on phytoplankton in the western tropical Atlantic Ocean off Barbados. Global Biogeochem. Cycles 30, 716–734.
Clark, C.M., Tilman, D., 2008. Loss of plant species after chronic low-level nitrogen deposition to prairie grasslands. Nature 451, 712–715.
Creamean, J.M., Suski, K.J., Rosenfeld, D., Cazorla, A., DeMott, P.J., Sullivan, R.C., White, A.B., Ralph, F.M., Minnis, P., Comstock, J.M., Tomlinson, J.M., Prather, K.A., 2013. Dust and biological aerosols from the sahara and Asia influence precipitation in the western U.S. Science 339, 1572–1578.
Fairlie, T.D., Jacob, D.J., Dibb, J.E., Alexander, B., Avery, M.A., van Donkelaar, A., Zhang, L., 2010. Impact of mineral dust on nitrate, sulfate, and ozone in transpacific Asian pollution plumes. Atmos. Chem. Phys. 10, 3999–4012.
Fang, Y., Yoh, M., Koba, K., Zhu, W., Takebayashi, Y., Xiao, Y., Lei, C., Mo, J., Zhang, W., Lu, X., 2011. Nitrogen deposition and forest nitrogen cycling along an urban-rural transect in southern China. Global Change Biol. 17, 872–885.
Flechard, C.R., Nemitz, E., Smith, R.I., Fowler, D., Vermeulen, A.T., Bleeker, A., Erisman, J.W., Simpson, D., Zhang, L., Tang, Y.S., Sutton, M.A., 2011. Dry deposition of reactive nitrogen to European ecosystems: a comparison of inferential models across the NitroEurope network. Atmos. Chem. Phys. 11, 2703–2728.
Forster, P., Ramaswamy, V., Artaxo, P., Berntsen, T., Betts, R., Fahey, D.W., Haywood, J., Lean, J., Lowe, D.C., Myhre, G., Nganga, J., Prinn, R., Raga, G., Schulz, M., Dorland, R.V., 2007. Changes in atmospheric constituents and in radiative forcing, climate change 2007: the physical science basis. In: Contribution of Working Group I to the Fourth Assessment Report of the Intergovernmental Panel on Climate Change. Cambridge University Press, Cambridge, United Kingdom and New York, NY, USA, pp. 129–234.
Fu, Q., Zhuang, G., Li, J., Huang, K., Wang, Q., Zhang, R., Fu, J., Lu, T., Chen, M., Wang, Q., Chen, Y., Xu, C., Hou, B., 2010. Source, long-range transport, and characteristics of a heavy dust pollution event in Shanghai. J. Geophys. Res. Atmos. 115.
Geng, H., Hwang, H., Liu, X., Dong, S., Ro, C.U., 2014. Investigation of aged aerosols in size-resolved Asian dust storm particles transported from Beijing, China, to Incheon, Korea, using low-Z particle EPMA. Atmos. Chem. Phys. 14, 3307–3323.
Higashi, T., Kambayashi, Y., Ohkura, N., Fujimura, M., Nakai, S., Honda, Y., Saijoh, K., Hayakawa, K., Kobayashi, F., Michigami, Y., Olando, A.E., Hitomi, Y., Nakamura, H., 2014. Effects of Asian dust on daily cough occurrence in patients with chronic cough: a panel study. Atmos. Environ. 92, 506–513.
Hu, W., Niu, H., Zhang, D., Wu, Z., Chen, C., Wu, Y., Shang, D., Hu, M., 2016. Insights into a dust event transported through Beijing in spring 2012: morphology, chemical composition and impact on surface aerosols. Sci. Total Environ. 565, 287–298.
Huang, X., Song, Y., Zhao, C., Cai, X., Zhang, H., Zhu, T., 2015. Direct radiative effect by multicomponent aerosol over China. J. Clim. 28, 3472–3495.
Jickells, T.D., An, Z.S., Andersen, K.K., Baker, A.R., Bergametti, G., Brooks, N., Cao, J.J., Boyd, P.W., Duce, R.A., Hunter, K.A., Kawahata, H., Kubilay, N., laRoche, J., Liss, P.S., Mahowald, N., Prospero, J.M., Ridgwell, A.J., Tegen, I., Torres, R., 2005. Global iron connections between desert dust, ocean biogeochemistry, and climate. Science 308, 67–71.
Kang, C.-H., Kim, W.-H., Ko, H.-J., Hong, S.-B., 2009. Asian dust effects on total suspended particulate (TSP) compositions at gosan in Jeju Island, Korea. Atmos. Res. 94, 345–355.
Karydis, V.A., Kumar, P., Barahona, D., Sokolik, I.N., Nenes, A., 2011. On the effect of dust particles on global cloud condensation nuclei and cloud droplet number. J. Geophys. Res. Atmos. 116.
Kumar, P., Sokolik, I.N., Nenes, A., 2009. Parameterization of cloud droplet formation for global and regional models: including adsorption activation from insoluble CCN. Atmos. Chem. Phys. 9, 2517–2532.
Lee, Y.G., Ho, C.-H., Kim, J.-H., Kim, J., 2015. Quiescence of Asian dust events in South Korea and Japan during 2012 spring: dust outbreaks and transports. Atmos. Environ. 114, 92–101.
Li, J., Wang, G., Ren, Y., Wang, J., Wu, C., Han, Y., Zhang, L., Cheng, C., Meng, J., 2016. Identification of chemical compositions and sources of atmospheric aerosols in Xi'an, inland China during two types of haze events. Sci. Total Environ. 566, 230–237.
Li, M., Wang, T., Han, Y., Xie, M., Li, S., Zhuang, B., Chen, P., 2017. Modeling of a severe dust event and its impacts on ozone photochemistry over the downstream Nanjing megacity of eastern China. Atmos. Environ. 160, 107–123.
Li, W.J., Shao, L.Y., 2009. Observation of nitrate coatings on atmospheric mineral dust particles. Atmos. Chem. Phys. 9, 1863–1871.
Li, W.J., Shao, L.Y., Shi, Z.B., Chen, J.M., Yang, L.X., Yuan, Q., Yan, C., Zhang, X.Y., Wang, Y.Q., Sun, J.Y., Zhang, Y.M., Shen, X.J., Wang, Z.F., Wang, W.X., 2014a. Mixing state and hygroscopicity of dust and haze particles before leaving Asian continent. J. Geophys. Res. Atmos. 119, 1044–1059.
Li, X., Cao, J., Chow, J., Han, Y., Lee, S., Watson, J., 2008. Chemical characteristics of carbonaceous aerosols during dust storms over Xi'an in China. Adv. Atmos. Sci. 25, 847–855.
Li, X., Feng, L., Huang, C., Yan, X., Zhang, X., 2014b. Potential hazardous elements (PHEs) in atmospheric particulate matter (APM) in the south of Xi'an during the dust episodes of 2001-2012 (NW China): chemical fractionation, ecological and health risk assessment. Environ. Earth Sci. 71, 4115–4126.
Li, X., Maring, H., Savoie, D., Voss, K., Prospero, J.M., 1996. Dominance of mineral dust in aerosol light-scattering in the North Atlantic trade winds. Nature 380, 416–419.
Liang, T., Tong, Y.a., Liu, X., Xu, W., Luo, X., Christie, P., 2016. High nitrogen deposition in an agricultural ecosystem of Shaanxi, China. Environ. Sci. Pollut. Res.

23, 13210–13221.
Liu, L., Zhang, X., Zhang, Y., Xu, W., Liu, X., Zhang, X., Feng, J., Chen, X., Zhang, Y., Lu, X., Wang, S., Zhang, W., Zhao, L., 2017. Dry particulate nitrate deposition in China. Environ. Sci. Technol. 51, 5572–5581.
Liu, X., Duan, L., Mo, J., Du, E., Shen, J., Lu, X., Zhang, Y., Zhou, X., He, C., Zhang, F., 2011. Nitrogen deposition and its ecological impact in China: an overview. Environ. Pollut. 159, 2251–2264.
Ma, Q., Liu, Y., Liu, C., Ma, J., He, H., 2012. A case study of Asian dust storm particles: chemical composition, reactivity to SO2 and hygroscopic properties. J. Environ. Sci. 24, 62–71.
Mahowald, N.M., Ballantine, J.A., Feddema, J., Ramankutty, N., 2007. Global trends in visibility: implications for dust sources. Atmos. Chem. Phys. 7, 3309–3339.
Meng, Z., Lu, B., 2007. Dust events as a risk factor for daily hospitalization for respiratory and cardiovascular diseases in Minqin, China. Atmos. Environ. Times 41, 7048–7058.
Mohan, S.M., 2016. An overview of particulate dry deposition: measuring methods, deposition velocity and controlling factors. Int. J. Environ. Sci. Te. 13, 387–402.
Nie, W., Wang, T., Xue, L.K., Ding, A.J., Wang, X.F., Gao, X.M., Xu, Z., Yu, Y.C., Yuan, C., Zhou, Z.S., Gao, R., Liu, X.H., Wang, Y., Fan, S.J., Poon, S., Zhang, Q.Z., Wang, W.X., 2012. Asian dust storm observed at a rural mountain site in southern China: chemical evolution and heterogeneous photochemistry. Atmos. Chem. Phys. 12, 11985–11995.
Niu, H., Zhang, D., Hu, W., Shi, J., Li, R., Gao, H., Pian, W., Hu, M., 2016. Size and elemental composition of dry-deposited particles during a severe dust storm at a coastal site of Eastern China. J. Environ. Sci. 40, 161–168.
Pan, X., Uno, I., Hara, Y., Kuribayashi, M., Kobayashi, H., Sugimoto, N., Yamamoto, S., Shimohara, T., Wang, Z., 2015. Observation of the simultaneous transport of Asian mineral dust aerosols with anthropogenic pollutants using a POPC during a long-lasting dust event in late spring 2014. Geophys. Res. Lett. 42, 1593–1598.
Pan, Y.P., Wang, Y.S., Tang, G.Q., Wu, D., 2012. Wet and dry deposition of atmospheric nitrogen at ten sites in Northern China. Atmos. Chem. Phys. 12, 6515–6535.
Seinfeld, J.H., Pandis, S.N., 1998. Atmospheric Chemistry and Physics: from Air Pollution to Climate Change. Wiley, USA.
Shen, Z., Cao, J., Arimoto, R., Han, Z., Zhang, R., Han, Y., Liu, S., Okuda, T., Nakao, S., Tanaka, S., 2009. Ionic composition of TSP and $PM_{2.5}$ during dust storms and air pollution episodes at Xi'an, China. Atmos. Environ. 43, 2911–2918.
Shi, J.H., Zhang, J., Gao, H.W., Tan, S.C., Yao, X.H., Ren, J.L., 2013. Concentration, solubility and deposition flux of atmospheric particulate nutrients over the Yellow Sea. Deep-Sea Res., Pt. II 97, 43–50.
Sun, Y., Zhuang, G., Huang, K., Li, J., Wang, Q., Wang, Y., Lin, Y., Fu, J.S., Zhang, W., Tang, A., Zhao, X., 2010. Asian dust over northern China and its impact on the downstream aerosol chemistry in 2004. J. Geophys. Res. Atmos. 115.
Sun, Y., Zhuang, G., Wang, Y., Han, L., Guo, J., Dan, M., Zhang, W., Wang, Z., Hao, Z., 2004. The air-borne particulate pollution in Beijing-concentration, composition, distribution and sources. Atmos. Environ. 38, 5991–6004.
Tang, M., Cziczo, D.J., Grassian, V.H., 2016. Interactions of water with mineral dust aerosol: water adsorption, hygroscopicity, cloud condensation, and ice nucleation. Chem. Rev. 116, 4205–4259.
Tang, M.J., Thieser, J., Schuster, G., Crowley, J.N., 2010. Uptake of NO3 and N2O5 to Saharan dust, ambient urban aerosol and soot: a relative rate study. Atmos. Chem. Phys. 10, 2965–2974.
Tao, Y., An, X., Sun, Z., Hou, Q., Wang, Y., 2012. Association between dust weather and number of admissions for patients with respiratory diseases in spring in Lanzhou. Sci. Total Environ. 423, 8–11.
Tsai, I.C., Chen, J.P., Lin, Y.C., Chou, C.C.K., Chen, W.N., 2015. Numerical investigation of the coagulation mixing between dust and hygroscopic aerosol particles and its impacts. J. Geophys. Res. Atmos. 120, 4213–4233.
Vet, R., Artz, R.S., Carou, S., Shaw, M., Ro, C.U., Aas, W., Baker, A., Bowersox, V.C., Dentener, F., Galy-Lacaux, C., Hou, A., Pienaar, J.J., Gillett, R., Cristina Forti, M., Gromov, S., Hara, H., Khodzher, T., Mahowald, N.M., Nickovic, S., Rao, P.S.P., Reid, N.W., 2014. A global assessment of precipitation chemistry and deposition of sulfur, nitrogen, sea salt, base cations, organic acids, acidity and pH, and phosphorus. Atmos. Environ. 93, 3–100.
Vitousek, P.M., Aber, J.D., Howarth, R.W., Likens, G.E., Matson, P.A., Schindler, D.W., Schlesinger, W.H., Tilman, D., 1997. Human alteration of the global nitrogen cycle: sources and consequences. Ecol. Appl. 7, 737–750.
Wang, F., Zhao, X., Gerlein-Safdi, C., Mu, Y., Wang, D., Lu, Q., 2017a. Global sources, emissions, transport and deposition of dust and sand and their effects on the climate and environment: a review. Front. Environ. Sci. Eng. 11.
Wang, F.J., Chen, Y., Guo, Z.G., Gao, H.W., Mackey, K.R., Yao, X.H., Zhuang, G.S., Paytan, A., 2017b. Combined effects of iron and copper from atmospheric dry deposition on ocean productivity. Geophys. Res. Lett. 44, 2546–2555.
Wang, G., Zhang, R., Gomez, M.E., Yang, L., Zamora, M.L., Hu, M., Lin, Y., Peng, J., Guo, S., Meng, J., Li, J., Cheng, C., Hu, T., Ren, Y., Wang, Y., Gao, J., Cao, J., An, Z., Zhou, W., Li, G., Wang, J., Tian, P., Marrero-Ortiz, W., Secrest, J., Du, Z., Zheng, J., Shang, D., Zeng, L., Shao, M., Wang, W., Huang, Y., Wang, Y., Zhu, Y., Li, Y., Hu, J., Pan, B., Cai, L., Cheng, Y., Ji, Y., Zhang, F., Rosenfeld, D., Liss, P.S., Duce, R.A., Kolb, C.E., Molina, M.J., 2016. Proc. Natl. Acad. Sci. U. S. A. 113, 13630–13635.
Wang, G.H., Cheng, C.L., Huang, Y., Tao, J., Ren, Y.Q., Wu, F., Meng, J.J., Li, J.J., Cheng, Y.T., Cao, J.J., Liu, S.X., Zhang, T., Zhang, R., Chen, Y.B., 2014. Evolution of aerosol chemistry in Xi'an, inland China, during the dust storm period of 2013-Part 1: sources, chemical forms and formation mechanisms of nitrate and sulfate. Atmos. Chem. Phys. 14, 11571–11585.
Wang, G.H., Li, J.J., Cheng, C.L., Zhou, B.H., Xie, M.J., Hu, S.Y., Meng, J.J., Sun, T., Ren, Y.Q., Cao, J.J., Liu, S.X., Zhang, T., Zhao, Z.Z., 2012. Observation of atmospheric aerosols at Mt. Hua and Mt. Tai in central and east China during spring 2009-Part 2: impact of dust storm on organic aerosol composition and size distribution. Atmos. Chem. Phys. 12, 4065–4080.
Wang, G.H., Zhou, B.H., Cheng, C.L., Cao, J.J., Li, J.J., Meng, J.J., Tao, J., Zhang, R.J., Fu, P.Q., 2013a. Impact of Gobi desert dust on aerosol chemistry of Xi'an, inland China during spring 2009: differences in composition and size distribution between the urban ground surface and the mountain atmosphere. Atmos. Chem. Phys. 13, 819–835.
Wang, L., Du, H., Chen, J., Zhang, M., Huang, X., Tan, H., Kong, L., Geng, F., 2013b. Consecutive transport of anthropogenic air masses and dust storm plume: two case events at Shanghai, China. Atmos. Res. 127, 22–33.
Wang, Y.Q., Zhang, X.Y., Draxler, R.R., 2009. TrajStat: GIS-based software that uses various trajectory statistical analysis methods to identify potential sources from long-term air pollution measurement data. Environ. Model. Software 24, 938–939.
Wu, F., Zhang, D., Cao, J., Guo, X., Xia, Y., Zhang, T., Lu, H., Cheng, Y., 2017. Limited production of sulfate and nitrate on front-associated dust storm particles moving from desert to distant populated areas in northwestern China. Atmos. Chem. Phys. 17, 14473–14484.
Wu, Y., Han, Z., Nazmi, C., Gross, B., Moshary, F., 2015. A trans-Pacific Asian dust episode and its impacts to air quality in the east coast of US. Atmos. Environ. 106, 358–368.
Xu, W., Luo, X.S., Pan, Y.P., Zhang, L., Tang, A.H., Shen, J.L., Zhang, Y., Li, K.H., Wu, Q.H., Yang, D.W., Zhang, Y.Y., Xue, J., Li, W.Q., Li, Q.Q., Tang, L., Lu, S.H., Liang, T., Tong, Y.A., Liu, P., Zhang, Q., Xiong, Z.Q., Shi, X.J., Wu, L.H., Shi, W.Q., Tian, K., Zhong, X.H., Shi, K., Tang, Q.Y., Zhang, L.J., Huang, J.L., He, C.E., Kuang, F.H., Zhu, B., Liu, H., Jin, X., Xin, Y.J., Shi, X.K., Du, E.Z., Dore, A.J., Tang, S., Collett Jr., J.L., Goulding, K., Sun, Y.X., Ren, J., Zhang, F.S., Liu, X.J., 2015. Quantifying atmospheric nitrogen deposition through a nationwide monitoring network across China. Atmos. Chem. Phys. 15, 12345–12360.
Yan, H., Liu, X., Qi, J., Gao, H., 2014. Dry deposition of PM_{10} over the yellow sea during asian dust events from 2001 to 2007. J. Environ. Sci. 26, 54–64.
Young, L.H., Li, C.H., Lin, M.Y., Hwang, B.F., Hsu, H.T., Chen, Y.C., Jung, C.R., Chen, K.C., Cheng, D.H., Wang, V.S., Chiang, H.C., Tsai, P.J., 2016. Field performance of a semi-continuous monitor for ambient PM2.5 water-soluble inorganic ions and gases at a suburban site. Atmos. Environ. 144, 376–388.
Zhang, H., McFarquhar, G.M., Cotton, W.R., Deng, Y., 2009. Direct and indirect impacts of Saharan dust acting as cloud condensation nuclei on tropical cyclone eyewall development. Geophys. Res. Lett. 36.
Zhang, X.Y., Arimoto, R., An, Z.S., 1997. Dust emission from Chinese desert sources linked to variations in atmospheric circulation. J. Geophys. Res. Atmos. 102, 28041–28047.
Zhao, J., Zhang, F., Xu, Y., Chen, J., Yin, L., Shang, X., Xu, L., 2011. Chemical characteristics of particulate matter during a heavy dust episode in a coastal city, Xiamen, 2010. Aerosol and Air Quality Research 11, 300–309.
Zhao, S., Yu, Y., Xia, D., Yin, D., He, J., Liu, N., Li, F., 2015. Urban particle size distributions during two contrasting dust events originating from Taklimakan and Gobi Deserts. Environ. Pollut. 207, 107–122.
Zimmermann, F., Weinbruch, S., Schuetz, L., Hofmann, H., Ebert, M., Kandler, K., Worringen, A., 2008. Ice nucleation properties of the most abundant mineral dust phases. J. Geophys. Res. Atmos. 113.